Journal of Materials Chemistry B

PAPER

View Article Online
View Journal | View Issue

Cite this: J. Mater. Chem. B, 2016, 4, 5418

Preparation of fluorescent Au–SiO_2 core–shell nanoparticles and nanorods with tunable silica shell thickness and surface modification for immunotargeting†

Prakash D. Nallathamby,*[a] Juliane Hopf,[b] Lisa E. Irimata,[a] Tracie L. McGinnity[a] and Ryan K. Roeder[a]

Received 5th July 2016,
Accepted 20th July 2016

DOI: 10.1039/c6tb01659f

www.rsc.org/MaterialsB

Gold–silica (Au–SiO_2) core–shell nanoparticles (NPs) enable multifunctional properties for *in vivo* biomedical applications. However, scalable synthesis methods are lacking for the preparation of Au–SiO_2 core–shell NPs less than 30 nm in overall diameter with a tunable silica shell less than 10 nm in thickness. Therefore, we prepared monodispersed Au–SiO_2 core–shell NPs less than 30 nm in overall diameter with a uniform, tunable silica shell ~1 to 14 nm in thickness using either citrate reduction followed by a modified Stöber method or oleylamine reduction followed by a reverse microemulsion method. Oleylamine reduction enabled up to 80-fold greater concentration yield compared to the citrate reduction method currently used for synthesizing Au core NPs. The formation of a tunable silica shell less than 10 nm in thickness was facilitated by controlling the molecular weight of the priming polymer (modified Stöber) or surfactant (reverse microemulsion) in addition to the concentration of the silane precursor, and was robust for encapsulating non-spherical morphologies such as Au nanorods. The reverse microemulsion method enabled several distinct advantages over the modified Stöber method, including greater control over the silica shell thickness, ~16-fold greater yield in core–shell NP concentrations for scalable synthesis, and the ability to encapsulate controlled concentrations of a molecular payload (*e.g.*, fluorophores with four different emission profiles) in the silica shell. Au–SiO_2 core–shell NPs were also bioconjugated with immunoglobulin-G (IgG) as a model antibody to demonstrate immunotargeting. Bioactivity of Au–SiO_2–IgG core–shell NPs was confirmed by agglomeration in the presence of protein A. The presence and proper orientation of IgG on NP surfaces was verified by direct observation in electron microscopy after negative staining. Therefore, the methods in this study for preparing and modifying Au–SiO_2 core–shell NPs provide a platform for engineering core–shell NPs with size-dependent functional properties for multispectral/multimodal imaging, drug delivery, and combined theranostics.

1. Introduction

Core–shell nanoparticles (NPs) possess unique functional material properties that are made possible by engineering the structure and composition of the core and shell.[1–3] The ability to combine different material compositions at the nanoscale has enabled new properties in core–shell NPs that are not possible with the core or shell composition alone.[1,2] Moreover, these properties can be tuned by independently tailoring the size and morphology of the core and shell. Core–shell NPs may also have multiple cores in a single shell or multiple shells on a single core.[2,4] For these reasons, core–shell NPs have found widespread applications in chromatography,[3,5] catalysis,[6–8] controlled drug or therapeutics delivery,[9–13] semiconductor photonics,[4,14,15] and diagnostic imaging probes and biosensors.[11,15–17]

For example, core–shell NPs have been used to conserve precious metals in catalysis by using an inexpensive core coated with a shell comprising the catalytic material.[7,8] The shell may also be used to form ordered porous structures to significantly increase the surface-to-volume ratio for catalysis and adsorption.[5] Quantum dots (QDs), which are core–shell semiconductor crystals, are used in solid state lasers, organic light emitting diode (OLED) displays, and LED lighting solutions.[14,15] The optical emissions and electronic properties of QDs can be tuned by controlling the shell thickness.[1,15] In biomedicine,

[a] Department of Aerospace and Mechanical Engineering, Bioengineering Graduate Program, University of Notre Dame, 145 Multidisciplinary Research Building, Notre Dame, IN 46556, USA. E-mail: pnallath@nd.edu; Tel: +1 574 631 5735
[b] Environmental Sciences Division, Oak Ridge National Laboratory, Oak Ridge, TN 37830, USA

† Electronic supplementary information (ESI) available. See DOI: 10.1039/c6tb01659f

core–shell NPs are advantageous to mitigate systemic toxicity by encapsulating a drug payload or imaging probe within an inert shell.[10–12] The shell surface chemistry can be further modified by molecular surface functionalization to promote colloidal stability and/or enable targeted delivery of the payload to the site of interest.[2,10–12,14–19] The overall size of core–shell NPs can be tailored by controlling the core size or shell thickness for colloidal stability, deliverability, and bioavailability.[18–22]

Gold–silica (Au–SiO_2) core–shell NPs have received particular attention in photonic[23–25] and biomedical[26–32] applications. Au NPs are well-known to exhibit strong absorption in the red and near infrared (NIR) spectral regions due to localized surface plasmon resonance (LSPR), enabling surface-enhanced Raman spectroscopy (SERS),[26–28] LSPR immunoassays,[29] and phototherapies.[30,31] Au NPs also exhibit strong absorption of X-rays, especially at high photon energies utilized in clinical computed tomography (CT), enabling contrast-enhanced CT.[32–34] Au NPs,[33–36] silica NPs,[37–39] and silica encapsulated NPs[30,40] 10–100 nm in diameter have exhibited at least 24 h blood circulation, a broad biodistribution, and low cytotoxicity at doses suitable for *in vivo* theranostic applications. Importantly, a silica shell can be used to encapsulate and thereby protect a payload (*e.g.*, fluorophores, photosensitive dyes, pharmaceuticals, NPs, *etc.*) from premature release due to enzymatic degradation or solubilization *in vivo*.[41] Moreover, the surface chemistry of silica is amenable to facile molecular surface modifications using silane linkages.[9,42] A number of studies have prepared Au–SiO_2 core–shell NPs,[24–26,28–30] but scalable synthesis methods and systematic investigations for controlling the silica shell thickness are limited, especially for NPs less than 30 nm in overall diameter with a silica shell less than 10 nm in thickness.[24,32,43–48]

Therefore, the objective of this study was to investigate scalable methods for the preparation of Au–SiO_2 core–shell NPs less than 30 nm in overall diameter with a tunable shell, 1 to 15 nm in thickness, which can be readily volume-loaded and/or surface functionalized with molecules for theranostic functions and targeted delivery. Monodispersed Au NP cores 14–16 nm in diameter were prepared by citrate and oleylamine reduction (Fig. 1). Oleylamine reduction enabled a one-pot synthesis with up to 80-fold greater concentration yield compared to the citrate reduction method currently used for synthesizing Au core NPs. The formation of a uniform, tunable silica shell, 1 to 15 nm in thickness, was investigated using either a modified Stöber method or water-in-oil reverse microemulsion method (Fig. 1). Uniform silica shell formation was also demonstrated on Au nanorod (NR) cores prepared by sodium borohydride reduction (Fig. 1). Fluorophores with four distinct emission profiles and varying molecular weight were encapsulated within the silica shell at controlled concentrations for multispectral and/or multimodal imaging, or as a proxy molecule to mimic a payload for drug delivery. Finally, Au–SiO_2 core–shell NPs were bioconjugated with rabbit immunoglobulin-G (IgG) to demonstrate immunotargeting. The presence and proper orientation of IgG on NP surfaces was verified by direct observation in electron microscopy after negative staining.

2. Materials and methods

Materials

Acetic acid ($C_2H_4O_2$, ACS grade, VWR, Batavia, IL), ammonium hydroxide (NH_4OH, 20%, VWR), (3-aminopropyl) triethoxysilane (APTES, $C_9H_{23}NO_3Si$, >98%, Sigma, St. Louis, MO), L-ascorbic acid ($C_6H_8O_6$, ≥99%, Sigma), cetyltrimethylammonium bromide (CTAB, $C_{19}H_{42}BrN$, ≥99%, Sigma), chloroauric acid ($AuCl_3 \cdot 3H_2O$, 99%, Sigma), citric acid ($C_6H_8O_7$, >99%, Sigma), cyclohexane (C_6H_{12}, 99%, Sigma), ethanol (95%, VWR), *N*,*N*′-diisopropylcarbodiimide (DIC, $C_7H_{14}N_2$, ≥98%, Sigma), dimethyl sulfoxide (DMSO, C_2H_6SO, >99.8%, VWR), DyLight™ 350 and 594 (98%, Fisher Scientific, Pittsburgh, PA), fluorescein isothiocyanate

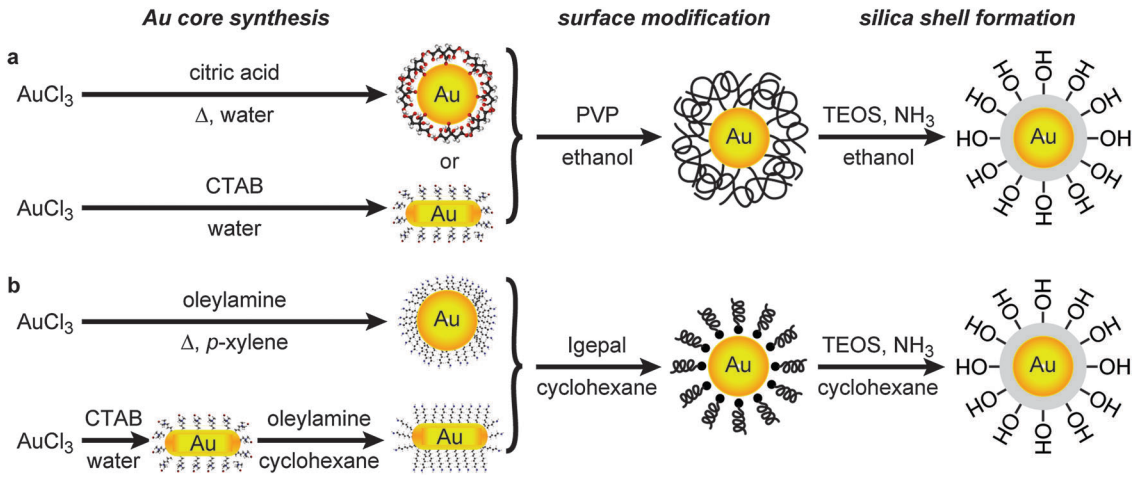

Fig. 1 Schematic diagram showing the stepwise synthesis of Au–SiO_2 core–shell NPs by two methods: (a) Au NP cores were synthesized *via* the citrate reduction method and the silica shell was prepared *via* the modified Stöber method using PVP as the polymeric surface primer. (b) Au NP cores were synthesized *via* the oleylamine reduction method and the silica shell was prepared *via* the reverse microemulsion method using the Igepal series of non-ionic detergents where micelles on the core NP surface acted as a soft template for silica shell formation. Note that the schematic is not drawn to scale.

(FITC, $C_{21}H_{11}NO_5S$, 90%, Sigma), *N*-hydroxysuccinimide (NHS, $C_4H_5NO_3$, 98%, Sigma), immunoglobulin-G (IgG, rabbit serum, ≥95%, Sigma), isopropanol (C_3H_7OH, Sigma), oleylamine ($C_{18}H_{35}NH_2$, 70%, Sigma), polyethylene glycol (PEG, $H(C_2H_4O)_nOH$, 12 K, Alfa Aesar, Ward Hill, MA), polyoxyethylene nonylphenylether ($(C_2H_4O)_n{\cdot}C_{15}H_{24}O$, Igepal®, CO-520, CO-720, CO-890, Sigma), polyvinylpyrrolidone (PVP, $(C_6H_9NO)_n$, PVP10, PVP40, PVP360, Sigma), rhodamine B isothiocyanate (RITC, $C_{29}H_{30}ClN_3O_3S$, Sigma), silver nitrate ($AgNO_3$, >99%, Sigma), sodium borohydride ($NaBH_4$, ≥96%, Sigma), tetraethylorthosilicate (TEOS, $C_8H_{20}O_4Si$, >99%, Sigma), (3-triethoxysilyl) propylsuccinic anhydride ($C_{13}H_{24}O_6Si$, 95%, Gelest, Morrisville, PA), and *p*-xylene (C_8H_{10}, ≥99%, Sigma) were all used as-received.

Au–SiO_2 core–shell NP synthesis *via* modified Stöber method (Fig. 1a)

Au NP synthesis *via* citrate reduction (Au–citrate NPs). 0.1 g $AuCl_3{\cdot}3H_2O$ was added to 400 ml of deionized (DI) water and the solution was boiled vigorously. A 1% solution of citric acid was added to the boiling solution under stirring at a 5 : 1 mass ratio of Au^{3+} to citrate ions and left boiling for an additional 20 min. The volume was then adjusted to a total of 500 ml using DI water and the solution was stirred overnight. The resulting solution of Au NPs had a Au^{3+} concentration of 0.5 mM and a wine red color.

Au NP stabilization with PVP (Au–PVP NPs). Au–citrate NPs were stabilized with PVP of three different molecular weights (PVP10: M_w = 10 000, PVP40: M_w = 40 000, PVP360: M_w = 360 000) to investigate the effect of the polymer shell molecular weight on the SiO_2 shell thickness. PVP was adsorbed to the surface of Au NPs by adding 1.5% or 0.25% w/v PVP to 500 ml of Au–citrate NPs in solution and stirring for 24 h at room temperature. The resulting Au–PVP NPs were thrice washed in ethanol and collected by centrifugation at 10 000 rcf, and were finally resuspended in 500 ml of ethanol.

Silica shell formation on Au–PVP NPs (Au–PVP–TEOS NPs). A 3 ml aliquot of Au–PVP NPs (~0.5 mM Au^{3+}) in ethanol was mixed with 3.5 ml of ethanol followed by 15 mM TEOS. Note that TEOS was always sourced from a stock solution that was stored at room temperature in a vacuum desiccator. 0.040 ml of 20% w/v NH_4OH was added rapidly under stirring and the solution was allowed to stir for 24 h at room temperature. The resulting Au–SiO_2 core–shell NPs were thrice washed in ethanol using centrifugation and were finally resuspended in 3 ml of ethanol.

Volume-loading fluorophores within Au–PVP–TEOS NPs. A 2 ml aliquot of Au–PVP40 NPs (~0.5 mM Au^{3+}) in ethanol was mixed with a 0.035 ml solution containing 0.65 mM APTES–FITC and 1.0 mM TEOS. 0.060 ml of 20% w/v NH_4OH was added rapidly under stirring and the solution was stirred for 24 h at room temperature. The resulting Au–SiO_2 core–shell NPs were thrice washed in ethanol using centrifugation and were finally resuspended in 3 ml of ethanol.

Au–SiO_2 core–shell NP synthesis *via* reverse microemulsion method (Fig. 1b)

Au NP synthesis *via* oleylamine reduction (Au–oleylNH_2 NPs). Oleylamine was added to 0.04 M $AuCl_3{\cdot}3H_2O$ in *p*-xylene at a molar ratio of 1 : 5 Au^{3+} to oleylamine. The solution was stirred for 1 h at 80 °C, refluxed for 6 h, and then cooled under stirring overnight. The resulting solution of Au–oleylNH_2 NPs was transferred to cyclohexane and had a Au^{3+} concentration of ~40 mM which was diluted to ~8–11 mM for subsequent steps.

Au NP stabilization with Igepal (Au–Igepal NPs). Au–oleylNH_2 NPs were stabilized with polyoxyethylene nonylphenylether (Igepal) at three different molecular weights (CO-520: M_n = 441, CO-720: M_n = 749, CO-890: M_n = 1982) to investigate the effect of the surfactant molecular weight on the SiO_2 shell thickness. 8.7 ml of Au–oleylNH_2 NPs (~8 mM Au^{3+}) in cyclohexane was diluted with 3.8 ml of cyclohexane. Igepal was added under ultrasonication to reach a final concentration of 0.165 M. Note that Igepal CO-890 is solid at room temperature; therefore, a solution of 0.165 M Igepal CO-890 in cyclohexane was heated to 60 °C for 15 min prior to use.

Silica shell formation on Au–Igepal NPs (Au–Igepal–TEOS NPs). A 12.5 ml aliquot of Au–Igepal NPs (~5.6 mM Au^{3+}) in cyclohexane was mixed with 22.5 mM TEOS under stirring. 0.210 ml of 20% w/v NH_4OH was added rapidly and the solution was allowed to stir for 24 h at room temperature. The resulting Au–SiO_2 core–shell NPs were thrice washed in isopropanol using centrifugation and were finally resuspended in 7.2 ml of ethanol.

Volume-loading fluorophores within Au–Igepal–TEOS NPs. An 8.7 ml aliquot of Au–oleylNH_2 NPs (~8 mM Au^{3+}) in cyclohexane was mixed with 3.8 ml of cyclohexane followed by the addition of 0.165 M Igepal CO-720. A 0.045 ml solution containing 0.65 mM APTES–FITC and 1.0 mM TEOS (1×) was added rapidly under stirring followed by 0.210 ml of 20% w/v NH_4OH. The APTES–FITC and TEOS concentrations were also increased by 5× and 10×. Volume-loading with RITC used a 0.073 ml solution containing 0.2 mM APTES–RITC and 0.7 mM TEOS (1×). Volume-loading with DyLight™ 350 or 594 used a 0.085 ml solution containing 0.57 mM APTES-DyLight™ 350 or 0.46 mM APTES-DyLight™ 594, respectively, and 1.0 mM TEOS (1×). In each case, 0.210 ml of 20% w/v NH_4OH was added after the fluorophore and the solution was allowed to stir for 24 h at room temperature. The resulting Au–SiO_2 core–shell NPs were thrice washed in isopropanol and collected by centrifugation at 10 000 rcf, and were finally resuspended in 7.2 ml of ethanol.

Au–SiO_2 core–shell NR synthesis *via* modified Stöber method (Fig. 1a)

Au NR synthesis *via* sodium borohydride reduction (Au–CTAB NRs). A 5 ml aliquot of 0.20 M CTAB was mixed with 5.0 ml of 0.5 mM $AuCl_3{\cdot}3H_2O$ in DI water. 0.60 ml of ice-cold 0.010 M $NaBH_4$ was added under stirring which resulted in the formation of a dark yellow solution. This seed solution was vigorously stirred for another 5 min and then allowed to stand at room temperature for subsequent use. A 5 ml aliquot of 0.20 M CTAB aqueous solution was added to 0.07 ml of 4.0 mM $AgNO_3$ in DI water at 30 °C. 5.0 ml of 1.0 mM $AuCl_3{\cdot}3H_2O$ in water was added and stirred for 5 min, followed by 0.0070 ml of 0.08 M ascorbic acid which turned the solution from dark yellow to colorless. Finally, 0.012 ml of the seed solution was added to this growth

solution at 27–30 °C and the solution color gradually changed within 10–20 min. The solution was allowed to stir overnight at 27–30 °C. The resulting solution of Au NRs had a Au^{3+} concentration of ~0.5 mM.

Au NR stabilization with PVP (Au–PVP NRs). 10 ml aliquots of 0.5 mM Au NRs were thrice washed in ethanol and collected by centrifugation at 10 000 rcf for 60 min, and were finally resuspended in 10 ml of 50/50 ethanol/water. Au-NRs were stabilized with PVP of two different molecular weights (PVP10: M_w = 10 000, PVP40: M_w = 40 000) to investigate the effect of the polymer shell molecular weight on the SiO_2 shell thickness. PVP was adsorbed to the surface of Au NPs by adding 1.5% w/v PVP to Au-NRs in solution and stirring for 24 h at room temperature. The resulting Au–PVP NRs were thrice washed in ethanol and collected by centrifugation at 10 000 rcf, and were finally resuspended in 10 ml of ethanol resulting in a Au^{3+} concentration of ~0.5 mM.

Silica shell formation on Au–PVP NRs (Au–PVP–TEOS NRs). A 1 ml aliquot of Au–PVP NRs (~0.5 mM Au^{3+}) in ethanol was mixed with 1.15 ml of ethanol followed by 15 mM TEOS. Note that TEOS was always sourced from a stock solution that was stored at room temperature in a vacuum desiccator. 0.040 ml of 20% w/v NH_4OH was added rapidly under stirring and the solution was allowed to stir for 24 h at room temperature. The resulting Au–SiO_2 core–shell NRs were thrice washed in ethanol using centrifugation and were finally resuspended in 1 ml of ethanol.

Au–SiO_2 core–shell NR synthesis *via* reverse microemulsion method (Fig. 1b)

Au NR stabilization with Igepal (Au–Igepal NRs). Au–CTAB NRs were synthesized *via* sodium borohydride reduction as described above for the modified Stöber method. 10 ml aliquots of 0.5 mM Au–CTAB NRs were thrice washed in cyclohexane and collected by centrifugation at 10 000 rcf for 60 min, and were finally resuspended in 1 ml of cyclohexane resulting in a Au^{3+} concentration of ~5 mM. The Au–CTAB NRs were stabilized by directly adding 0.010 ml of Igepal CO-520 under ultrasonication for a final concentration of 0.2 M Igepal CO-520. Alternatively, oleylamine was added to ~5 mM Au–CTAB NRs prior to Igepal at a molar ratio of 1 : 5 Au^{3+} to oleylamine and stirred for at least 12 h to allow for ligand exchange and displacement of CTAB on Au NR surfaces by oleylamine. Au–oleylNH_2 NRs were thrice washed in cyclohexane and collected by centrifugation at 10 000 rcf for 60 min, and were finally resuspended in 1 ml of cyclohexane resulting in a Au^{3+} concentration of ~5 mM. The Au–oleylNH_2 NRs were then stabilized by adding 0.012 ml of Igepal CO-720 under ultrasonication for a final concentration of 0.2 M Igepal CO-720.

Silica shell formation on Au–Igepal NRs (Au–Igepal–TEOS NRs). A 1 ml aliquot of Au–Igepal NRs (~5 mM Au^{3+}) in cyclohexane was mixed with 22.5 mM TEOS under rapid stirring. 0.021 ml of 20% w/v NH_4OH was added rapidly and the solution was allowed to stir for 24 h at room temperature. The resulting Au–SiO_2 core–shell NRs were thrice washed in isopropanol using centrifugation and were finally resuspended in 7.2 ml of ethanol.

Antibody bioconjugation to Au–Igepal–TEOS NPs

A 10 ml aliquot of 8 mM Au–Igepal–TEOS NPs in 90% ethanol in DI water was mixed with 100 μl of 3-(triethoxysilyl) propylsuccinic anhydride under rapid stirring, sealed, and stirred for at least 12 h at room temperature before adding 20 ml of 1% acetic acid in DI water. The solution was stirred for an additional 12 h to ensure complete hydrolysis of succinic anhydride (SA) to succinic acid and then mixed with 20 ml of isopropanol to bring the total volume to 50 ml. The resulting Au–Igepal–TEOS–SA NPs were thrice collected by centrifugation at 10 000 rcf for 60 min and resuspended in DI water under ultrasonication (model 500, Fisher Scientific) for 10 s at 25% amplitude pulsed for 1 s on and 0.7 s off. The NPs were finally resuspended in 7.2 ml of DI water to yield 10 mM Au–Igepal–TEOS–SA NPs.

A 0.5 ml aliquot of 10 mM Au–Igepal–TEOS–SA NPs was freeze-dried (FreeZone Triad, Labconco Inc., Kansas City, MO), purged with dry nitrogen, and transferred into a dry box under nitrogen. The freeze-dried pellet of Au–Igepal–TEOS–SA NPs was resuspended in 2 ml of anhydrous DMSO with vigorous pipetting. 15 μl of DIC and 0.015 g of NHS were added and stirred for 24 h to activate the carboxylic acid group on the NPs through the formation of an NHS ester. The resulting NHS ester activated Au–Igepal–TEOS–SA NPs in DMSO were mixed under stirring with 2 ml of 0.05 mg ml^{-1} rabbit serum IgG in 1% w/v PEG buffered in PBS at pH 7.2. The solution was stirred for 30 min at room temperature and 12 h at 4 °C. The resulting bioconjugated Au–Igepal–TEOS–SA–IgG NPs were thrice washed in 10 mM phosphate buffered solution (PBS), pH 7.2 containing 1% w/v PEG, using centrifugation and were resuspended in 2 ml PBS resulting in a final concentration of ~2.5 mM Au–Igepal–TEOS–SA–IgG NPs.

Characterization of Au–SiO_2 core–shell NPs

The size and morphology of the Au–SiO_2 core–shell NPs were characterized using transmission electron microscopy (TEM, 2011T, JEOL, Tokyo, Japan) at an accelerating voltage of 200 kV. Specimens were prepared by pipetting 10 μl drops from NP solutions onto carbon-coated grids and evaporating the solvent under partial vacuum. The mean (±standard deviation) Au NP core diameter, Au NR core aspect ratio, SiO_2 shell thickness, and their size distributions were measured for at least 100 particles sampled from digital images at 50 000–100 000× magnification (ImageJ v1.49, National Institutes of Health). The composition of the NP core and shell was verified using an energy dispersive X-ray spectroscopy (EDS) detector (INCA, Oxford Instruments, Abingdon, UK) with a 75 s exposure time.

Volume-loading of fluorophores in the SiO_2 shell was characterized by epifluorescence microscopy (Eclipse ME600, Nikon Instruments, Melville, NY) using filters for FITC (excitation = 460–500 nm, emission = 510–560 nm), RITC (excitation = 530–550 nm, emission = 590–650 nm), DyLight™ 350 (excitation = 352–402 nm, emission = 417–477 nm), and DyLight™ 594 (excitation = 562–602 nm, emission = 624–664 nm). Dark field images of Au NPs and Au–SiO_2 core–shell NPs were acquired

using a dark field oil immersion condenser (N.A. = 1.43–1.20, Nikon) to show localized surface plasmon resonance of the NPs. Fluorescence and dark field images were recorded using a digital camera equipped with a red-green-blue filter for true color imaging (QIClick™, QImaging, Surrey, BC).

The presence and orientation of IgG conjugated to the surface of Au–SiO_2 core–shell NPs was imaged by TEM after staining grids with methylamine vanadate (NanoVan®, Nanoprobes, Yaphank, NY). The bioactivity of IgG conjugated NPs was confirmed using an agglomeration assay after mixing 100 μl of Au–Igepal–TEOS–SA–IgG NPs with a 0.01% w/v solution of heat-inactivated, formalin-fixed *Staphylococcus aureus* cells which overexpress protein A on the cell wall (PANSORBIN™, EMD Millipore, Billerica, MA).[49]

3. Results and discussion

Synthesis of Au NP cores

Citrate reduction. The reduction of gold(III) chloride by citrate ions under refluxing conditions produced highly stable, well-dispersed Au NPs in aqueous solution with a mean diameter of 14.2 ± 1.7 nm (Fig. 2a). The coefficient of variation (CV) in size was 12% which indicated a narrow distribution where 91% of NPs were 12–17 nm in diameter. Citrate reduction is well-known to produce monodispersed Au NPs due to a favorable combination of nucleation, growth, and equilibration to prevent coalescence and broadening of the size distribution.[50–52] However, the concentration yield with respect to Au^{3+} ions was at most ~0.5 mM which is up to 100-fold less than the concentrations typically utilized for *in vivo* delivery.[34] Thus, the synthesis of Au NPs by the citrate reduction method is highly reproducible, but not sufficiently scalable. A 10 ml solution of 50 mM Au NPs requires that at least a 1 L stock solution is prepared and subsequently concentrated by repeated centrifugation.

Oleylamine reduction. Au NPs were also prepared by oleylamine reduction in a non-polar solvent. Oleylamine is a long-chain primary alkylamine which can act as an electron donor at elevated temperatures, thereby serving as both a reducing agent and surfactant.[53,54] The reduction of gold(III) chloride by oleylamine (oleylNH_2) in *p*-xylene under refluxing conditions produced highly stable, well-dispersed Au NPs with a mean diameter of 16.2 ± 2.3 nm (Fig. 2b). NPs exhibited a dodecahedral morphology (Fig. 2b) likely due to the C=C double bond in the middle of oleylamine coordinating Au^{3+} ions and directing NP growth. The CV in size was 14% which indicated a narrow distribution where 89% of NPs were 15–19 nm in diameter. Thus, Au NPs prepared by oleylamine reduction exhibited a size distribution that was comparable to the citrate reduction method.

The preparation of Au NPs by oleylamine reduction in a non-polar solvent exhibited two distinct advantages compared with citrate reduction in an aqueous solvent. First, the concentration yield for the oleylamine reduction method with respect to Au^{3+} ions was ~40 mM, which is up to 80-fold greater than that for citrate reduction, due to the greater stability of oleylamine as a capping agent compared with citrate ions, and thus requires little or no subsequent concentration by centrifugation. Second, Au–oleylNH_2 NPs were prepared in a non-polar solvent (*p*-xylene) and were therefore readily redispersed in a non-polar solvent (cyclohexane) which was subsequently used as the oil phase in the reverse microemulsion method for preparing core–shell NPs (Fig. 1b). The preparation of monodispersed core–shell NPs with a 1 : 1 incorporation of Au NP cores in the silica shell requires no aggregation of Au NP cores in the oil phase of the reverse microemulsion. TEM micrographs clearly showed that Au NPs prepared by oleylamine reduction were well-separated and non-aggregated (Fig. 2b).

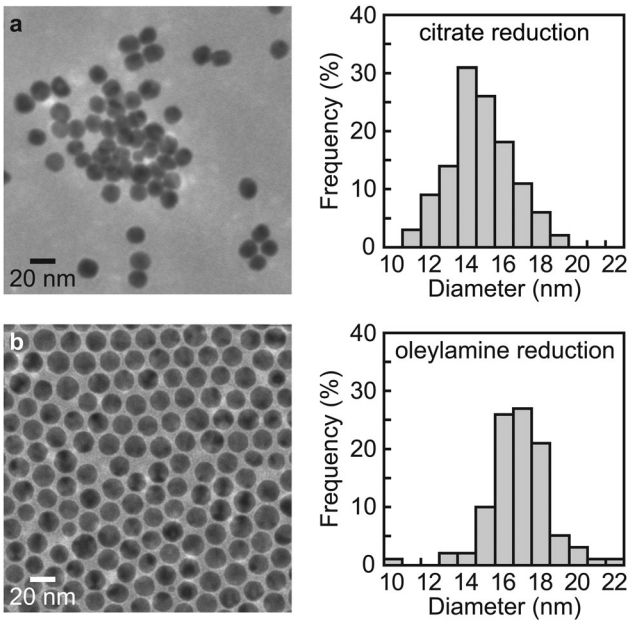

Fig. 2 Representative TEM micrographs and measured NP size distributions for Au NP cores synthesized by (a) the citrate reduction method, which exhibited a mean (±standard deviation) diameter of 14.2 ± 1.7 nm, and (b) the oleylamine reduction method, which exhibited a mean diameter of 16.2 ± 2.3 nm.

Synthesis of Au–SiO_2 core–shell NPs

Modified Stöber method. A modified Stöber method[32,55,56] was used to encapsulate Au NPs prepared by the citrate reduction method in a silica shell (Fig. 1a). Amphiphilic, ethanol dispersible Au NPs were first created by surface modification with PVP of varying molecular weight to displace citrate ions from Au NP surfaces and act as a primer for silica condensation. Au–PVP NPs were subsequently introduced as seeds or templates for the rapid hydrolysis of alkyl silicates in alcoholic solutions using ammonium hydroxide as a base catalyst, followed by the rapid condensation of silane precursors to form Au–SiO_2 core–shell NPs.

Au–SiO_2 core–shell NPs were prepared with a silica shell thickness ranging from ~1 to 3.5 nm by varying the molecular weight and concentration of PVP (Fig. 3). The Au core and silica shell were able to be visualized in TEM micrographs as darker and lighter, respectively, due to the greater electron density of Au (Fig. 3). The composition of the Au core and silica shell was

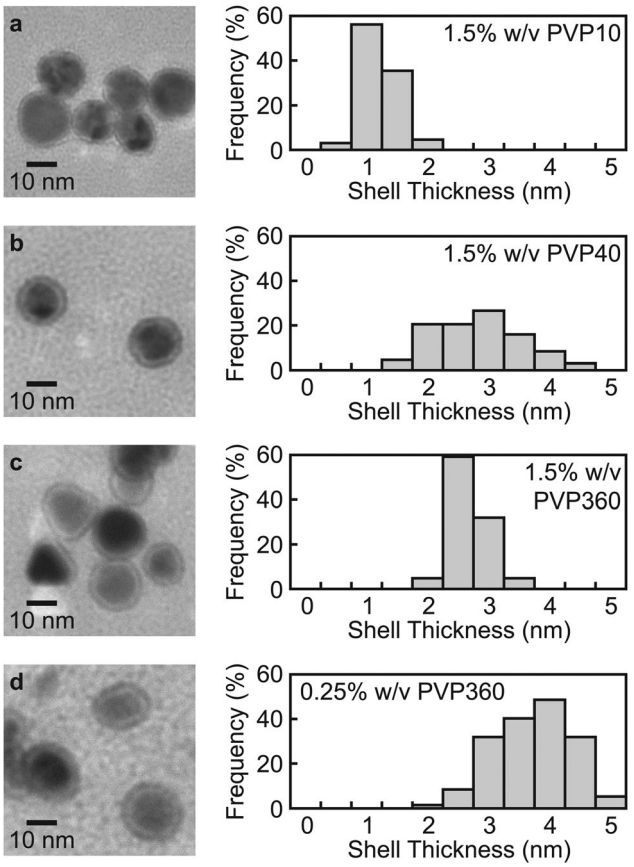

Fig. 3 Representative TEM micrographs showing the effect of the molecular weight and concentration of PVP on the measured silica shell thickness of Au–SiO_2 core–shell NPs prepared by the modified Stöber method. The Au core and silica shell are visibly darker and lighter, respectively, due to the greater electron density of Au. Au–SiO_2 NPs synthesized using (a) 1.5% w/v PVP10, (b) 1.5% w/v PVP40, (c) 1.5% w/v PVP360, and (d) 0.25% w/v PVP360 resulted in a mean (±standard deviation) silica shell thickness of 1.0 ± 0.3, 2.6 ± 0.8, 2.5 ± 0.3, and 3.5 ± 0.6 nm, respectively.

also verified by EDS (Fig. S1a, ESI†). Au–SiO_2 core–shell NPs synthesized using 1.5% w/v PVP10, 1.5% w/v PVP40, 1.5% w/v PVP360, and 0.25% w/v PVP360 exhibited a mean silica shell thickness of 1.0 ± 0.3, 2.6 ± 0.8, 2.5 ± 0.3, and 3.5 ± 0.6 nm, respectively (Fig. 3). At a constant concentration of 1.5% w/v PVP, the silica shell thickness was increased for PVP40 compared with PVPV10, but did not increase further for PVP360 (Fig. 3a–c). However, decreasing the concentration to 0.25% w/v PVP360 produced an increase in the silica shell thickness (Fig. 3c and d). This result suggests that a high molecular weight and high concentration of PVP may have acted to entangle Au NPs and hinder condensation of silica on Au NP surfaces. These results also established the importance of optimizing both the priming polymer molecular weight and concentration for tailoring the silica shell thickness. The optimum concentration of TEOS for these PVP concentrations was determined to be 15 mM TEOS. Under these conditions, greater than 99% of the NPs observed in TEM micrographs (Fig. 3) were core–shell NPs and less than 1% were non-core–shell Au NPs or SiO_2 NPs. At concentrations greater than 15 mM TEOS (2–10×), increasing amounts of amorphous silica formed as a white precipitate in addition to Au–SiO_2 core–shell NPs, which prohibited reliable synthesis of a silica shell of greater thickness.

The modified Stöber method is a robust, well-established, and highly reproducible process. The silica shell composition is readily controlled by the mixture of silane precursors added before the condensation step. Excess silane precursors or amorphous silica in solution can be removed by washing the NPs in alcohol using ultra-centrifugation or filtration. In previous studies, the silica shell has been tailored from ~10 to 100 nm in thickness by adjusting the silane precursor concentration, catalyst concentration, or reaction time,[24,32,43–47] which govern the rate of silane hydrolysis, rate of silane condensation, and amount of growth, respectively. In this study, the silica shell was able to be tailored from ~1 to 3.5 nm in thickness by tuning the priming polymer molecular weight and concentration. Thus, the overall diameter of core–shell NPs was only ~7 to 20% greater than the diameter of the cores, which could be advantageous for engineering core–shell NPs with size-dependent functional properties. However, the preparation of Au–SiO_2 core–shell NPs by the modified Stöber method yielded ~0.5 mM concentrations with respect to Au^{3+} ions and is thus limited by tedious and time-consuming steps required to scale-up the necessary concentrations for use as a potential theranostic.

Reverse microemulsion method. A reverse microemulsion method was used to encapsulate Au NPs prepared by the oleylamine reduction method in a silica shell (Fig. 1b). A non-ionic surfactant (Igepal) of varying molecular weight was used to form water-in-oil reverse microemulsion micelles in cyclohexane. Hydrophobic Au–oleylNH_2 NPs were stabilized in the oil phase by the micelles prior to becoming hydrophilic during the condensation of silane precursors on the NP surfaces to form Au–SiO_2 core–shell NPs.

Au–SiO_2 core–shell NPs were prepared with a silica shell thickness ranging from ~2.5 to 14 nm by varying the Igepal molecular weight and silane precursor concentration (Fig. 4). The Au core and silica shell were able to be visualized in TEM micrographs as darker and lighter, respectively, due to the greater electron density of Au (Fig. 4). The composition of the Au core and silica shell was also verified by EDS (Fig. S1b, ESI†). Au–SiO_2 core–shell NPs synthesized using 1X TEOS (22.5 mM) with Igepal CO-520, CO-720, and CO-890 exhibited a mean silica shell thickness of 14.0 ± 2.6, 2.6 ± 0.5 and 2.4 ± 0.4 nm, respectively (Fig. 4). Au–SiO_2 core–shell NPs synthesized using Igepal CO-720 with 1×, 1.5×, 2×, and 2.5× TEOS exhibited a mean silica shell thickness of 2.6 ± 0.5, 3.8 ± 0.7, 4.0 ± 0.7, and 10.0 ± 2.4 nm, respectively. Thus, the silica shell thickness was increased by a decreased Igepal molecular weight and increased TEOS concentration. A decrease in the surfactant molecular weight is known to increase the number of surfactant molecules in each micelle,[57] which would be expected to decrease the stability of micelles and promote transport of reactants into micelle, resulting in the formation of a greater silica shell thickness.

The optimum concentration of Igepal and Au–oleylNH_2 NPs for achieving a high yield of core–shell NPs was determined to

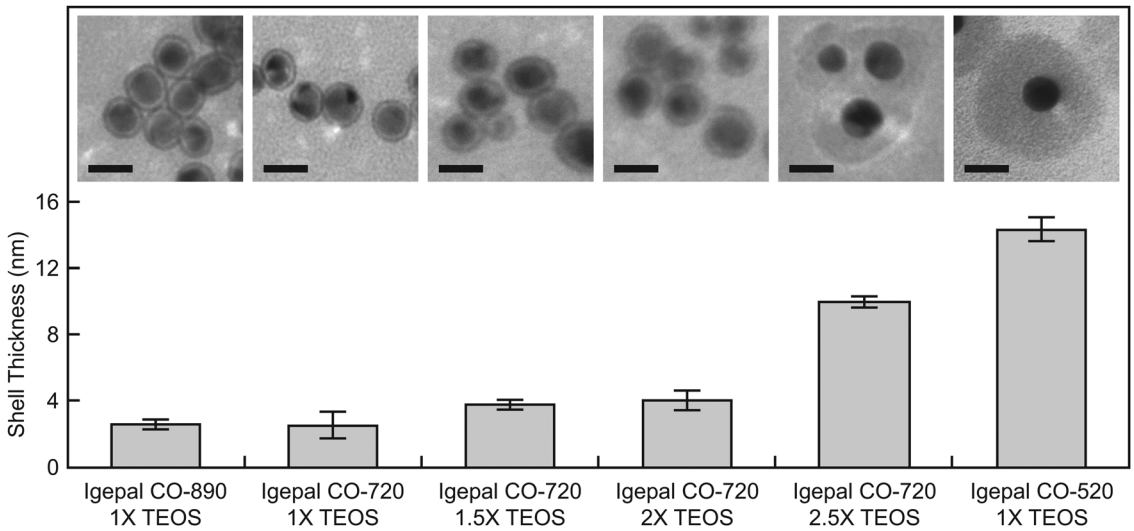

Fig. 4 Representative TEM micrographs showing the effects of the molecular weight of Igepal and the TEOS concentration on the measured silica shell thickness of Au–SiO_2 NPs prepared by the reverse microemulsion method. The Au core and silica shell are visibly darker and lighter, respectively, due to the greater electron density of Au. Scale bars = 20 nm. Error bars show one standard deviation of the mean. The mean (±standard deviation) silica shell thickness from left to right was 2.4 ± 0.4, 2.6 ± 0.5, 3.8 ± 0.7, 4.0 ± 0.7, 10.0 ± 2.4, and 14.0 ± 2.6 nm. Note that the concentration of Igepal was held constant at 0.165 M for each preparation and 1× TEOS corresponded to 22.5 mM TEOS.

be 0.165 M and ~8 mM (Au^{3+}) in cyclohexane, respectively, and were thus held constant for all reported syntheses. Under these conditions, greater than 99% of the NPs observed in TEM micrographs (Fig. 4) were core–shell NPs and less than 1% were non-core–shell Au NPs or SiO_2 NPs. In contrast, Au–oleylNH_2 NP concentrations less than 5 mM or greater than 10 mM with respect to Au^{3+} ions resulted in poor incorporation of Au NPs into silica shells (Fig. S2, ESI†).

The silica shell was able to be tailored from ~2.5 to 14 nm in thickness, such that Au–SiO_2 core–shell NPs were ~15 to 30 nm in overall diameter, which could be advantageous for engineering core–shell NPs with size-dependent functional properties. In contrast, Au–SiO_2 core–shell NPs prepared in previous studies have been typically greater than 30 nm in overall diameter due to a silica shell greater than 10 nm in thickness.[24,32,43–47] The ability to reliably encapsulate NPs within a thin silica shell less than 10 nm in thickness, as demonstrated in this study, carries important implications for tailoring the dose of a molecular payload encapsulated in the shell and/or the controlling the release of a drug payload as the silica shell degrades, as both are dependent on the shell thickness. In other words, a thin silica shell is potentially useful for rapidly delivering a precise dose to a site of interest.

The preparation of Au–SiO_2 core–shell NPs by the reverse microemulsion exhibited three distinct advantages compared with the modified Stöber method. First, the reverse microemulsion method enabled greater control over the silica shell thickness (~2 to 14 nm) compared with the modified Stöber method (~1 to 3.5 nm). Second, the reverse microemulsion method was more scalable as the NP concentration was ~8 mM with respect to Au^{3+} ions, which was ~16-fold greater than that for the modified Stöber method where the concentration yield with respect to Au^{3+} ions was only ~0.5 mM. This scalability and the use of inexpensive industrial-grade oleylamine suggests that the methods in this study may be readily translated to pilot-scale production. Third, the reverse microemulsion method permitted the use of silane precursor concentrations up to one order of magnitude greater than that for the modified Stöber method. Therefore, the reverse microemulsion method enabled the encapsulation of a molecular payload in the silica shell over a wide concentration range, as demonstrated below.

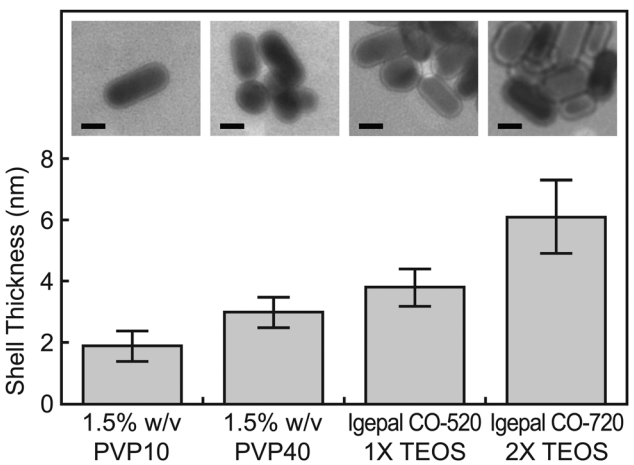

Fig. 5 Representative TEM micrographs showing the effects of the molecular weight of PVP and Igepal, as well as the TEOS concentration, on the measured silica shell thickness of Au–SiO_2 NRs prepared by the modified Stöber and reverse microemulsion method, respectively. The Au core and silica shell are visibly darker and lighter, respectively, due to the greater electron density of Au. Scale bars = 20 nm. Error bars show one standard deviation of the mean. The mean (±standard deviation) silica shell thickness from left to right was 1.9 ± 0.5, 3.0 ± 0.5, 3.8 ± 0.6 and 6.1 ± 1.2 nm. Note that the concentration of Igepal were held constant at 0.2 M for each preparation and 1× TEOS corresponded to 22.5 mM TEOS.

Synthesis of Au–SiO_2 core–shell NRs

Au NRs were also encapsulated in a silica shell to demonstrate conformal shell formation on non-spherical NPs using either the modified Stöber or reverse microemulsion method (Fig. 1). Au NR cores were prepared by established methods using sodium borohydride as a reducing agent.[58] As-prepared Au NRs were highly stable and well-dispersed with a mean aspect ratio of 3.6 ± 0.2. Au–SiO_2 core–shell NRs synthesized by the modified Stöber method using ~0.5 mM Au–CTAB NRs with 1.5% w/v PVP10 and 1.5% w/v PVP40 exhibited a mean silica shell thickness of 1.9 ± 0.5 and 3.0 ± 0.5 nm, respectively (Fig. 5). Au–SiO_2 core–shell NRs synthesized by the reverse microemulsion method using ~5 mM Au–CTAB NRs with 0.2 M Igepal CO-520, and Au–oleylNH_2 NRs with 0.2 M Igepal CO-720, both with 22.5 mM TEOS, exhibited a mean silica shell thickness of 3.8 ± 0.6 and 6.1 ± 1.2 nm, respectively (Fig. 5). Cuboidal Au–SiO_2 core–shell NPs were also synthesized by the reverse microemulsion method using Igepal CO-720 with 1×, 1.5×, 2×, and 2.5× TEOS and exhibited a mean silica shell thickness of 3.2 ± 0.6, 4.4 ± 0.1, 5.7 ± 0.7 and 8.0 ± 0.9 nm, respectively (Fig. S3, ESI†). Therefore, the methods in this study were robust for encapsulating various NP morphologies[25,28–31] in a uniform silica shell of tunable thickness. Moreover, the reverse microemulsion method was again advantageous in enabling a greater control over the silica shell thickness (Fig. 5 and Fig. S3, ESI†) and ~10-fold greater concentration yield compared to the modified Stöber method.

Fluorescent labeling of Au–SiO_2 core–shell NPs

After demonstrating the ability to tailor the silica shell thickness from ~1 to 14 nm, fluorophores were encapsulated within the silica shell to demonstrate control over a molecular payload. FITC was readily incorporated in Au–PVP–TEOS core–shell NPs prepared by the modified Stöber method, but controlled volume-loading was not investigated due to the limited ability to tailor the silica shell thickness.

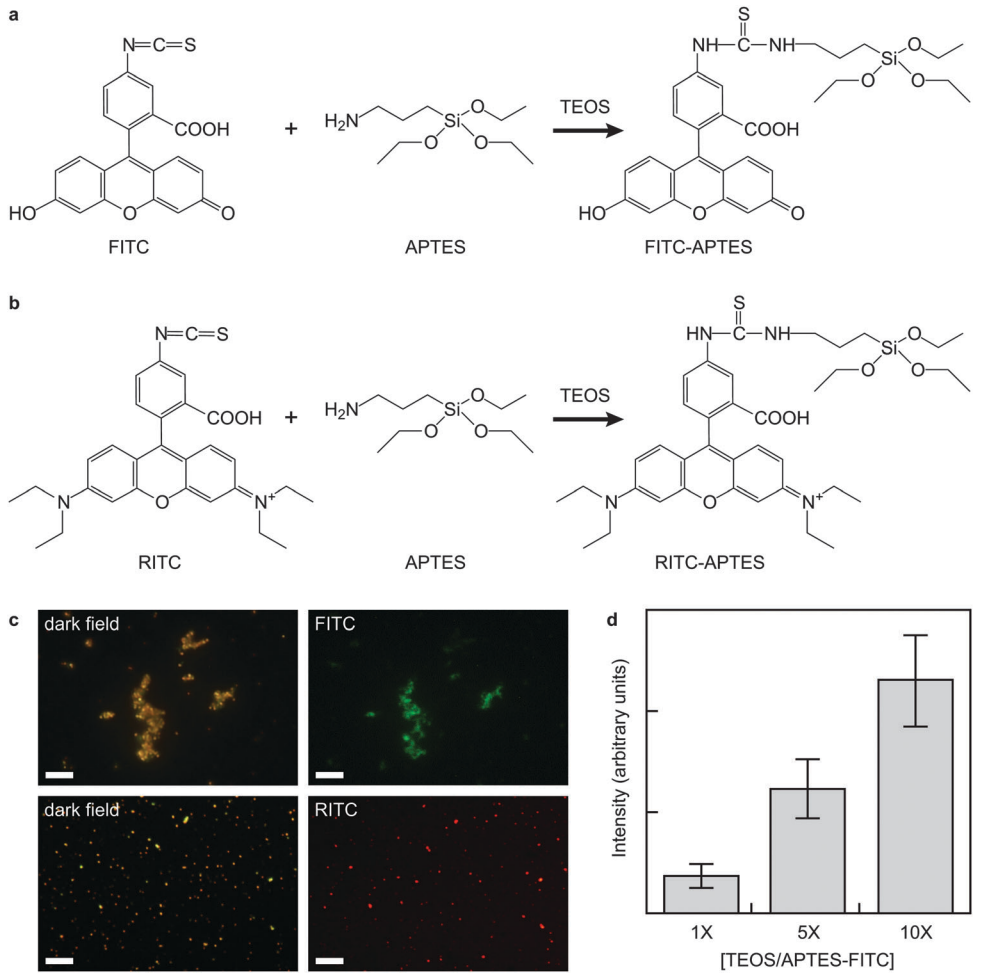

Fig. 6 Au–SiO_2 core–shell NPs prepared using the reverse microemulsion method were volume-loaded with (a) FITC and (b) RITC by linking to APTES using isothiocyanate chemistry. (c) Dark field (left) and epifluorescence (right) micrographs showing corresponding LSPR and fluorescence emission (FITC = green, RITC = red), respectively, from Au–SiO_2 core–shell NPs labeled with FITC and RITC. Scale bars = 10 μm. (d) The fluorescence signal intensity increased linearly with the concentration of the TEOS/APTES–FITC precursor. Error bars show one standard deviation of the distribution mean. Note that 1× TEOS/APTES–FITC corresponded to 1 mM TEOS and 0.65 mM APTES–FITC.

Therefore, Au–Igepal–TEOS core–shell NPs prepared by the reverse microemulsion method were volume-loaded with controlled concentrations of FITC and RITC (Fig. 6). The amine group on APTES was conjugated to either FITC (Fig. 6a) or RITC (Fig. 6b) and added to Au–Igepal NPs (~8 mM Au^{3+}) along with TEOS at a TEOS : APTES molar ratio of 20 : 13 or 7 : 2, respectively, to yield either Au–Igepal–TEOS/APTES–FITC (green fluorescence) or Au–Igepal–TEOS/APTES–RITC (red fluorescence) core–shell NPs. The incorporation of FITC and RITC in the silica shell was verified by comparing dark field and epifluorescence micrographs of Au–SiO_2 core–shell NPs, which showed corresponding LSPR and fluorescence emission (FITC = green, RITC = red), respectively (Fig. 6c). In addition to FITC and RITC, two proprietary fluorophores, DyLight™ 350 and DyLight™ 594, were also volume-loaded in the silica shell of Au–SiO_2 core–shell NPs to demonstrate a multispectral, multimodal imaging platform (Fig. S4, ESI†).

The ability to tailor a molecular payload *via* the silica shell thickness was investigated by preparing Au–SiO_2 core–shell NPs using Igepal CO-720 with 1×, 5×, and 10× TEOS/APTES–FITC (1× = 1 mM TEOS and 0.65 mM APTES–FITC). The fluorescence signal intensity increased linearly with the concentration of the TEOS/APTES–FITC precursor (Fig. 6d) indicating that the molecular payload in the silica shell was able to be tailored. The number of FITC molecules per NP was estimated by calculation to be 968, 1621 and 7299 for a mean silica shell thickness of ~2.5, 4, and 10 nm, respectively.

The ability to control the number of various molecules loaded in the silica shell of core–shell NPs is important for multispectral and/or multimodal imaging. Four different fluorophores with distinct emission profiles were readily encapsulated into the silica shell enabling multispectral imaging (Fig. S4, ESI†). Volume-loading of various fluorophores within a silica shell of tunable thickness enabled control over the fluorescence signal intensity (Fig. 6d), as well as protection against photobleaching and quenching from solvent and solute effects.[16,41] Volume-loading was estimated to enable the incorporation of a 10-fold greater number of fluorophores compared to surface conjugation for a 10 nm silica shell on a 16 nm Au core (Fig. S5, S6 and Table S1, ESI†). Thus, the volume-loading approach in this study is superior to covalently linking fluorophores to the surface of the silica shell, as employed previously.[32,48,59] Au–SiO_2 core–shell NPs can also be used as a trimodal contrast agent in *in vivo* and *in vitro* imaging due to the strong absorption of X-rays by gold in CT,[32–34] the LSPR of gold in NIR imaging/assays,[26–29] and volume-loading fluorophores in the silica shell for epifluorescence (Fig. 6c).

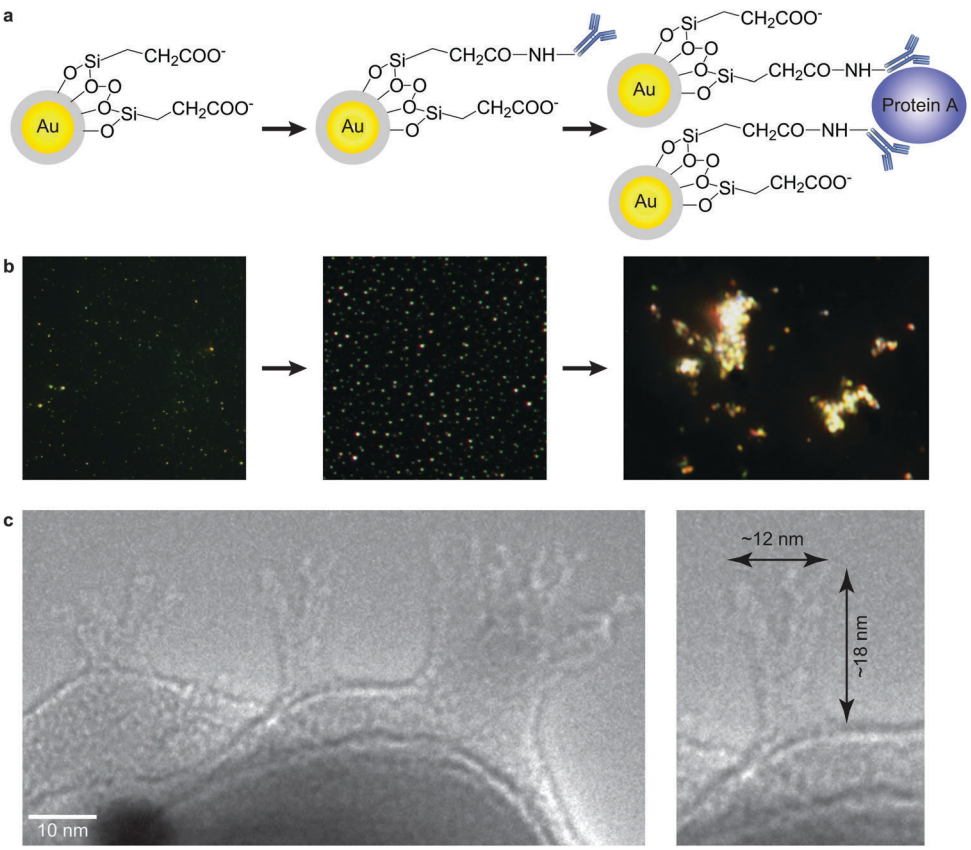

Fig. 7 Au–SiO_2 core–shell NPs prepared using the reverse microemulsion method were (a) bioconjugated with rabbit IgG using carbodiimide/succinimide chemistry and bioactivity was demonstrated by binding to protein A overexpressed on the cell wall of formalin-fixed *Staphylococcus aureus* cells (PANSORBIN™). (b) Dark field micrographs showed (left to right) well-dispersed Au–SiO_2 core–shell NPs after activation and bioconjugation with IgG, followed by agglomeration and removal from solution in the presence of protein-A. (c) TEM micrograph of the surface of bioconjugated Au–SiO_2–IgG core–shell NPs confirming the presence and proper orientation of Y-shaped IgG antibodies which were negatively stained (NanoVan®).

Moreover, the platform in this study could be readily extended to utilize a paramagnetic NP cores (*e.g.*, Fe_3O_4 or Gd_2O_3) for magnetic resonance imaging[11,16,42] or to incorporate radiopharmaceuticals in the silica shell for nuclear imaging.[42]

Au–SiO_2 core–shell NPs can also be used as a drug delivery vehicle or combined theranostic.[16,30] In this study, four fluorophores of varying molecular weight – FITC (389 g mol^{-1}), RITC (536 g mol^{-1}), DyLight™ 350 (874 g mol^{-1}), and DyLight™ 594 (1078 g mol^{-1}) – served as a proxy for small molecule (<1100 g mol^{-1}) drugs such as cisplatin (300 g mol^{-1}) and doxorubicin (543 g mol^{-1}). Controlled loading of a drug payload in the silica shell is critical for controlling the drug dose and release rate. The demonstrated ability to reliably encapsulate a molecular payload within a silica shell ~1 to 14 nm in thickness suggests potential utility for controlled delivery of a precise dose to a site of interest. Moreover, the platform presented in this study could be readily extended to utilize the Au NP core or incorporate a photosensitive dye in the silica shell for photothermal and photodynamic therapies.[16,30,31] Importantly, volume-loading a molecular payload within the silica shell also leaves the shell surface available for conjugation strategies to enable targeted delivery, as demonstrated below.

Antibody bioconjugation to Au–SiO_2 core–shell NPs

Immunoglobulin-G (IgG) derived from rabbit serum was covalently linked to Au–Igepal–TEOS–SA NPs using carbodiimide/succinimide chemistry (Fig. 7a) to demonstrate a robust platform for immunotargeting imaging probes or therapeutics. The bioactivity of the Au–SiO_2–IgG NPs was investigated using a heat-inactivated, formalin-fixed strain of *Staphylococcus aureus*, a bacterial strain which overexpresses protein A on the cell wall.[49] Dark field imaging revealed that Au–SiO_2–IgG NPs agglomerated out of solution in the presence of protein A (Fig. 7b), which qualitatively confirmed the presence, tertiary structure, and bioactivity of IgG on NP surfaces. Importantly, the presence and proper orientation of Y-shaped antibodies on Au–SiO_2–IgG NPs was directly observed for the first time in TEM micrographs after negative staining (Fig. 7c). Measured dimensions of ~18 × 12 nm (Fig. 7c) agreed with unit cell dimensions measured from X-ray crystallography and electron microscopy.[60] The demonstrated ability to control the orientation of bioconjugated antibodies such that the two antigen binding sites are facing away from the surface of the NP is crucial for immunotargeting antigens in therapeutic, diagnostic imaging, and biosensing applications. Moreover, the approach used in this study is readily transferrable to other high affinity antibodies, since the vast majority of the antibodies exist as Y-shaped monomers.[61]

4. Conclusions

Au–SiO_2 core–shell NPs were prepared by (a) citrate reduction followed by a modified Stöber method or (b) oleylamine reduction followed by a reverse microemulsion method. Monodispersed Au–SiO_2 core–shell NPs less than 30 nm in overall diameter were reliably prepared with a uniform, tunable silica shell ~1 to 14 nm in thickness on Au NP cores 14–16 nm in diameter. The formation of a tunable silica shell less than 10 nm in thickness was facilitated by controlling the molecular weight of the priming polymer (modified Stöber) or surfactant (reverse microemulsion) in addition to the concentration of the silane precursor. The methods in this study were also demonstrated to be robust for encapsulating non-spherical NPs (*e.g.*, Au nanorods) in a uniform, conformal silica shell less than 10 nm in thickness. The reverse microemulsion method enabled several distinct advantages over the modified Stöber method, including greater control over the silica shell thickness, ~16-fold greater yield in NP concentrations for scalable one-pot synthesis, and the ability to encapsulate controlled concentrations of a molecular payload (*e.g.*, fluorophores) in the silica shell. Fluorophores with four distinct emission profiles and varying molecular weight were readily encapsulated into the silica shell at controlled concentrations for multispectral and/or multimodal imaging, or as a proxy molecule to mimic a payload for drug delivery. Au–SiO_2 core–shell NPs were also bioconjugated IgG as a model antibody to demonstrate immunotargeting. Bioactivity of Au–SiO_2–IgG core–shell NPs was confirmed by agglomeration in the presence of protein A. The presence and proper orientation of IgG on NP surfaces was verified by direct observation in electron microscopy after negative staining. Therefore, the methods in this study for preparing and modifying Au–SiO_2 core–shell NPs, provides a broad platform in general, for engineering core–shell NPs with size-dependent functional properties for multimodal imaging, drug delivery, and combined theranostics.

Conflict of interest

We have no conflict of interest to declare.

Acknowledgements

This work was supported by grants from the National Science Foundation (NSF DMR-1309587), Walther Cancer Foundation (Advanced Basic Cancer Research Grant), and Defense Advanced Research Projects Agency (DARPA-14-56-A2P-PA-055). The authors acknowledge the Notre Dame Integrated Imaging Facility (NDIIF) for the use of the TEM and Center for Environmental Science and Technology (CEST) for the use of ICP-OES.

References

1 S. Wei, Q. Wang, J. Zhu, L. Sun, H. Lin and Z. Guo, *Nanoscale*, 2011, **3**, 4474.
2 R. Ghosh Chaudhuri and S. Paria, *Chem. Rev.*, 2012, **112**, 2373.
3 R. Hayes, A. Ahmed, T. Edge and H. Zhang, *J. Chromatogr. A*, 2014, **1357**, 36.
4 P. Bajwa, F. Gao, A. Nguyen, B. Omogo and C. D. Heyes, *ChemPhysChem*, 2016, **17**, 731.
5 D. Zhao, J. Feng, Q. Huo, N. Melosh, G. H. Fredrickson, B. F. Chmelka and G. D. Stucky, *Science*, 1998, **279**, 548.
6 C. J. Zhong and M. M. Maye, *Adv. Mater.*, 2001, **13**, 1507.
7 S. U. Son, Y. Jang, J. Park, H. B. Na, H. M. Park, H. J. Yun, J. Lee and T. Hyeon, *J. Am. Chem. Soc.*, 2004, **126**, 5026.

8 P. Venkatesan and J. Santhanalakshmi, *Langmuir*, 2010, **26**, 12225.
9 I. I. Slowing, B. G. Trewyn, S. Giri and S.-Y. Lin, *Adv. Funct. Mater.*, 2007, **17**, 1225.
10 L. Zhang, F. X. Gu, J. M. Chan, A. Z. Wang, R. S. Langer and O. C. Farokhzad, *Clin. Pharmacol. Ther.*, 2008, **83**, 761.
11 S. Laurent, D. Forge, M. Port, A. Roch, C. Robic, L. Vander Elst and R. N. Muller, *Chem. Rev.*, 2008, **108**, 2064.
12 R. C. Mundargi, V. R. Babu, V. Rangaswamy, P. Patel and T. M. Aminabhavi, *J. Controlled Release*, 2008, **125**, 193.
13 E. Yan, Y. Ding, C. Chen, R. Li, Y. Hu and X. Jiang, *Chem. Commun.*, 2009, 2718.
14 P. M. Allen, W. Liu, V. P. Chauhan, J. Lee, A. Y. Ting, D. Fukumura, R. K. Jain and M. G. Bawendi, *J. Am. Chem. Soc.*, 2010, **132**, 470.
15 M. Geszke-Moritz and M. Moritz, *Mater. Sci. Eng., C*, 2013, **33**, 1008.
16 M. De, P. S. Ghosh and V. M. Rotello, *Adv. Mater.*, 2008, **20**, 4225.
17 R. Torres Martin de Rosales, R. Tavare, A. Glaria, G. Varma, A. Protti and P. J. Blower, *Bioconjugate Chem.*, 2011, **22**, 455.
18 F. Caruso, *Adv. Mater.*, 2001, **13**, 12.
19 J. V. Jokerst, T. Lobovkina, R. N. Zare and S. S. Gambhir, *Nanomedicine*, 2011, **6**, 715.
20 I. ul Haq and E. Matijevic, *J. Colloid Interface Sci.*, 1997, **192**, 104.
21 X. Son, R. Rossin, J. L. Turner, M. L. Becker, M. J. Joralemon, M. J. Welch and K. L. Wooley, *Biomacromolecules*, 2005, **6**, 2541.
22 S. Hirn, M. Semmler-Behnke, C. Schleh, A. Wenk, J. Lipka, M. Schaffler, S. Takenaka, W. Moller, G. Schmid, U. Simon and W. G. Kreyling, *Eur. J. Pharm. Biopharm.*, 2011, **77**, 407.
23 T. Ung, L. M. Liz-Marzan and P. Mulvaney, *J. Phys. Chem. B*, 2001, **105**, 3441.
24 Y. Lu, Y. Yin, Z.-Y. Li and Y. Xia, *Nano Lett.*, 2002, **2**, 785.
25 X. D. Wang, A. P. Luo, H. Liu, N. Zhao, M. Liu, Y. F. Zhu, J. P. Xue, Z. C. Luo and W. C. Xu, *Opt. Express*, 2015, **23**, 22602.
26 S. P. Mulvaney, M. D. Musick, C. D. Keating and M. J. Natan, *Langmuir*, 2003, **19**, 4784.
27 C. L. Zavaleta, B. R. Smith, I. Walton, W. Doering, G. Davis, B. Shajaei, M. J. Natan and S. S. Gambhir, *Proc. Natl. Acad. Sci. U. S. A.*, 2008, **106**, 13511.
28 L. Rodriguez-Lorenzo, Z. Krpetic, S. Barbosa, R. A. Alvarez-Puebla, L. M. Liz-Marzan, I. A. Prior and M. Brust, *Integr. Biol.*, 2011, **3**, 922.
29 M. J. Banholzer, N. Harris, J. E. Millstone, G. C. Schatz and C. A. Mirkin, *J. Phys. Chem. C*, 2010, **114**, 7521.
30 P. Huang, L. Bao, C. Zhang, J. Lin, T. Luo, D. Yeng, M. He, Z. Li, G. Gao, B. Gao, S. Fu and D. Cui, *Biomaterials*, 2011, **32**, 9796.
31 P. Vijayaraghavan, C. H. Liu, R. Vankayala, C. S. Chiang and K. C. Hwang, *Adv. Mater.*, 2014, **26**, 6689.
32 Y. Kobayashi, H. Inose, T. Nakagawa, K. Gonda, M. Takeda, N. Ohuchi and A. Kasuyo, *J. Colloid Interface Sci.*, 2011, **358**, 329.
33 L. E. Cole, T. Vargo-Gogola and R. K. Roeder, *ACS Nano*, 2015, **9**, 8923.
34 L. E. Cole, R. D. Ross, J. M. Tilley, T. Vargo-Gogola and R. K. Roeder, *Nanomedicine*, 2015, **10**, 321.
35 N. Khlebtsov and L. Dykman, *Chem. Soc. Rev.*, 2011, **40**, 1647.
36 A. M. Alkilany and C. J. Murphy, *J. Nanopart. Res.*, 2010, **12**, 2313.
37 T. Liu, L. Li, X. Teng, X. Huang, H. Liu, D. Chen, J. Ren, J. He and F. Tang, *Biomaterials*, 2011, **32**, 1657.
38 Q. He and J. Shi, *J. Mater. Chem.*, 2011, **21**, 5845.
39 F. Tang, L. Li and D. Chen, *Adv. Mater.*, 2012, **24**, 1504.
40 J. S. Kim, T. J. Yoon, K. N. Yu, B. G. Kim, S. J. Park, H. W. Kim, K. H. Lee, S. B. Park, J. K. Lee and M. H. Cho, *Toxicol. Sci.*, 2006, **89**, 338.
41 W. Wang, P. D. Nallathamby, C. M. Foster, J. L. Morrell-Falvey, N. P. Mortensen, M. J. Doktycz, B. Gu and S. T. Retterer, *Nanoscale*, 2013, **5**, 10369.
42 P. D. Nallathamby, N. P. Mortensen, H. A. Palko, M. Malfatti, C. Smith, J. Sonnett, M. J. Doktycz, B. Gu, R. K. Roeder, W. Wang and S. T. Retterer, *Nanoscale*, 2015, **7**, 6545.
43 L. M. Liz-Marzán, M. Giersig and P. Mulvaney, *Langmuir*, 1996, **12**, 4329.
44 E. Mine, A. Yamada, Y. Kobayashi, M. Konno and L. M. Liz-Marzan, *J. Colloid Interface Sci.*, 2003, **264**, 385.
45 Y. L. Shi and T. Asefa, *Langmuir*, 2007, **23**, 9455.
46 J. Ye, B. Van de Broek, R. De Palma, W. Libaers, K. Clays, W. Van Roy, G. Borgh and G. Maes, *Colloids Surf., A*, 2008, **322**, 225.
47 N. R. Jana, C. Earhart and J. Y. Ying, *Chem. Mater.*, 2007, **19**, 5074.
48 A. Vanderkooy, Y. Chen, F. Gonzaga and M. A. Brook, *ACS Appl. Mater. Interfaces*, 2011, **3**, 3942.
49 S. W. Kessler, *J. Immunol.*, 1975, **115**, 1617.
50 J. Turkevich, P. C. Stevenson and J. Hillier, *Discuss. Faraday Soc.*, 1951, **11**, 55.
51 L. M. Browning, K. J. Lee, T. Huang, P. D. Nallathamby, J. E. Lowman and X.-H. N. Xu, *Nanoscale*, 2009, **1**, 138.
52 Z. Zhang, R. D. Ross and R. K. Roeder, *Nanoscale*, 2011, **2**, 582.
53 C. Shen, C. Hui, T. Yang, C. Xiao, J. Tian, L. Bao, S. Chen, H. Ding and H. Gap, *Chem. Mater.*, 2008, **20**, 6939.
54 S. Mourdikoudis and L. M. Liz-Marzán, *Chem. Mater.*, 2013, **25**, 1465.
55 W. Stöber, A. Fink and E. Bohn, *J. Colloid Interface Sci.*, 1968, **26**, 62.
56 M. Behara and S. Ram, *Appl. Nanosci.*, 2013, **3**, 83.
57 J. M. Neugebauer, *Methods Enzymol.*, 1990, **182**, 239.
58 D. K. Smith and B. A. Korgel, *Langmuir*, 2008, **24**, 644.
59 P. Reineck, D. Gomez, S. H. Ng, M. Karg, T. Bell, P. Mulvaney and U. Bach, *ACS Nano*, 2013, **7**, 6636.
60 V. R. Sarma, E. W. Silverton, D. R. Davies and W. D. Terry, *J. Biol. Chem.*, 1971, **246**, 3753.
61 W. Wang, S. Singh, D. L. Zeng, K. King and S. Nema, *J. Pharm. Sci.*, 2007, **96**, 1.

